Supporting Information

Understanding Metal Synergy in Heterodinuclear Catalysts for the Copolymerization of CO_2 and Epoxides

Arron C. Deacy,[a] Alexander F.R. Kilpatrick,[a] Anna Regoutz[b] and Charlotte K. Williams[a]*

[a]Department of Chemistry, University of Oxford, Chemistry Research Laboratory, 12 Mansfield Road, Oxford, *OX1 3TA, UK.*

[b]*Department of Materials, Imperial College London, London, SW7 2AZ, U.K.*

**Corresponding author: charlotte.williams@chem.ox.ac.uk*

Experimental Section.....2-5
Figure 1: MALDI-ToF mass spectrum of **MgCo**. 6
Figure 2: FT-IR spectra of a) **CoCo**, b) **MgMg** and c) **MgCo**.....6
Figure 3: X-ray Photoelectron Spectra and Discussion 7
Figure 4: SQUID Magnetic data for **MgCo** and **CoCo** and Discussion 8-10
Figure 5: Cyclic voltammagrams and Oxidation Potentials of **MgMg**, **MgCo**, **CoCo**.....11
Table 1: Electrode Potentials vs. Ferrocene for **MgMg**, **MgCo**, **CoCo**.....11
Table 2: CO_2/CHO Copolymerization Data with and without 1,2-Cyclohexane diol (Discussion). ...12-13
Figure 6: ^{1}H NMR spectra of **MgCo** before and after heating to 120 °C for 24 h in d_8-dioxane.....14
Figure 7: Molecular structures of other highly active 1 bar CO_2/CHO catalysts.....14
Figure 8: Copolymerization kinetic data 15
Figure 9: Reaction kinetic data; order in [**MgCo**].....16
Figure 10: Kinetic analysis of ROCOP of CO_2/CHO using 1.67 mM MgCo in DEC (100 °C, 1 bar).....17
Figure 11. Proposed mechanisms for initiation (a), propagation (b) and chain-transfer (c). 17
Figure 12: Molecular structures of other highly active CO_2/CHO catalysts. 18
Figure 13: ^{1}H NMR spectrum of the product resulting from attempted **MgCo** oxidation.....19
Figure 14. Temperature dependence of copolymerization rates. 20
Table 4: Data obtained from an Eyring analysis, linear fits and calculated rate coefficients for the copolymerization of CHO/CO_2 with **MgCo**.....21
Table 5: Data obtained from an Eyring analysis, linear fits and calculated rate coefficients for the copolymerization of CHO/CO_2 with **CoCo**.....21
Table 6: Data obtained from an Eyring analysis, linear fits and calculated rate coefficients for the copolymerization of CHO/CO_2 with **MgMg**.....21
Figure 15: Eyring plots (ln(k/T) vs 1/T) for **MgCo** (a), **CoCo** (b) and **MgMg** (c).....22
Table 7: Transition state thermodynamic parameters, $\Delta H^{\ddagger}$ and $\Delta S^{\ddagger}$..... 22
Table 8: CO_2/other epoxide ROCOP using **MgCo**.....23
Figure 16: Representative examples of a) GPC and b) ^{1}H NMR spectra of the crude polymers. 23
References.....23-24

Experimental Section

Materials: Solvents and reagents were obtained from commercial sources and used as received unless stated otherwise. THF and pentane were obtained from an SPS system, degassed by several freeze-pump-thaw cycles and further dried with 3 Å molecular sieves and stored under nitrogen. Cyclohexene oxide was dried over calcium hydride overnight and purified via fractional distillation prior to use and stored in an inert atmosphere. Research-grade carbon dioxide was used for copolymerization studies. All sample preparations were carried out in nitrogen filled glovebox. The pro-ligand (H_2L), **MgMg** and **CoCo** were synthesised by literature procedures.[1-3]

*Synthesis of **MgCo***: $Mg(N(SiMe_3)_2)_2$ (0.75 g, 2.17 mmol) and $Co(OAc)_2$ (0.39 g, 2.17 mmol) was added to a solution of H_2L (1.20 g, 2.17 mmol) in THF (10 mL) and heated to 100 °C in a sealed ampoule for 16 h. The solvent was reduced in *vacuo* to dryness and the solid washed with pentane (3 x 10 mL) to afford a pale pink solid (1.12 g, 1.49 mmol, 69 %). MS (MALDI-ToF): m/z 693 $[LMgCo(OAC)]^+$. Elemental Analysis for $C_{38}H_{60}CoMgN_4O_6$ (751.37 $gmol^{-1}$): Calculated; C, 60.68; H, 8.04; N, 7.45 %. Found; C, 60.51; H, 7.88; N, 7.20 %.

Methods:

Gel permeation chromatography analysis: carried out on a two mixed bed PSS SDV linear S column in series, with THF as the eluent at a flow rate of 1mL/min on a Shimadzu LC-20AD instrument at 40 °C. Polymer Molecular Mass (M_n) was determined by comparison against polystyrene standards. The polymer samples were dissolved in HPLC-grade THF (10 mg/mL) and filtered through a 0.20 μm porous filter frit prior to analysis.

Elemental Analysis: determined by Stephen Boyer at London Metropolitan University.

Mass Spectroscopy (MALDI-ToF): The spectra were measured on a Micromass MALDI micro MX spectrometer. The Matrix was *trans*-2-[3-(4-tert-butylphenyl)-2-methyl-2-propenylidene]-malonitrile. The samples were prepared by mixing 10 mg/mL THF solutions of complex and matrix together. This mixture (2 μL) was then spotted on the MALDI-plate and allowed to dry under an inert atmosphere.

X-ray Photoelectron Spectroscopy (XPS): The surface of the catalyst powders were characterised using X-ray photoelectron spectroscopy (XPS). The spectra were recorded on a Thermo Scientific K-Alpha^{+} X-ray photoelectron spectrometer operating at $2x10^{-9}$ mbar base pressure. This system incorporates a monochromated, microfocused Al Kα X-ray source (hν = 1486.6 eV) and a 180° double focusing hemispherical analyser with a 2D detector. The X-ray source was operated a 6 mA emission current and 12 kV anode bias and a flood gun was used to minimize sample charging. Data were collected at 20 eV pass energy using an X-ray spot size of 400 μm. All data were analysed using the Avantage software package.

Superconducting Quantum Interference Device (SQUID) magnetometry: Magnetic measurements on powdered samples were carried out using a Quantum Design MPMS-5 magnetometer at a field of 0.1 Tesla and different temperatures (2 – 300 K). Weighed samples (ca. 30 mg) were placed into gelatine capsules and then loaded into nonmagnetic plastic straw before entering the cryostat. Data reproducibility was checked using two independently synthesised (and measured) samples. Values of the magnetic susceptibility were corrected for the underlying diamagnetic increment by using tabulated Pascal constants,[4] per bimetallic complex unit for **MgCo** ($\chi_{dia} = -4.76 \times 10^{-4}$ cm^3 mol^{-1}) and **CoCo** ($\chi_{dia} = -4.83 \times 10^{-4}$ cm^3 mol^{-1}). The mass magnetic susceptibility, χ_g, was

multiplied by the molar mass for **MgCo** (752.2 g mol^{-1}) and **CoCo** (786.8 g mol^{-1}) to obtain the magnetic susceptibility per mole of bimetallic complex, χ_m.

Cyclic voltammetry (CV): Electrochemical studies were carried out using a PalmSens EmStat Blue potentiostat under computer control. Cyclic voltammetry experiments were performed in a MBraun UNIlab glovebox under N_2 using a three-electrode configuration with a Au disc (2.0 mm^2) as the working electrode, a Pt wire as the counter electrode and a Ag wire as the pseudo-reference electrode. Sample solutions were prepared by dissolving the analyte (*ca.* 5 mM) in THF (10.0 cm^3) followed by addition of a supporting electrolyte [^{n}Bu$_4$N][PF$_6$]. The reported mid-peak potentials are referenced internally to that of the Fc$^+$/Fc redox couple, which was measured by adding ferrocene (*ca*. 1 mg) to the sample solution.

Low pressure copolymerizations: A solution of catalyst (16 μmol) in epoxide (33 mmol) in diethylcarbonate (total volume 10 mL) was added to a Schlenk tube, under nitrogen. The reaction was subjected to five vacuum/CO_2 cycles (pressure regulated at 1 bar CO_2). The Schlenk was fitted with a DiComp probe for *insitu*-IR spectroscopic measurements and submerged into an oil bath pre-heated to the appropriate temperature. At this point the REACTIR instrument was set to begin data-collection (t_0). It is notable that all catalysts show some short induction period and that the relative lengths are independent of catalyst type. Typical induction periods were 20 mins @ 80°C, 15 mins @ 100°C and 10 mins @ 120 °C. It is noted that this time period incorporates the time required for the reaction solution to reach the desired temperature (from room temperature).

High pressure copolymerizations: A solution of catalyst (16 μmol) in epoxide (33 mmol) in diethylcarbonate (total volume 10 mL) was injected into a 100 mL Parr reactor fitted with a DiComp sentinel probe for *insitu*-IR spectroscopic measurements. The reactor was

then pressurised with CO_2 to the targeted reaction pressure and allowed to reach the required temperature.

Mass Spectrometry and Infrared Spectroscopy

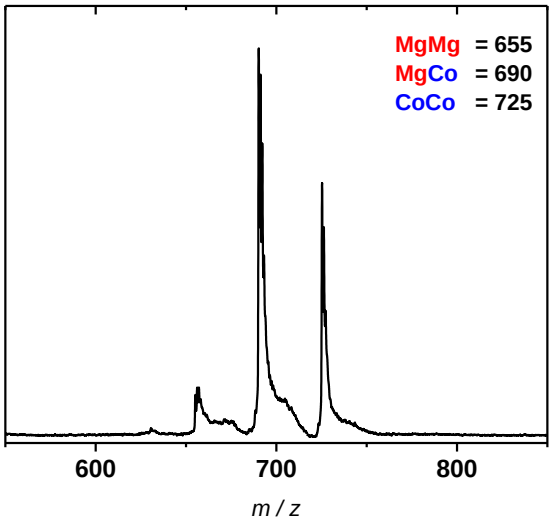
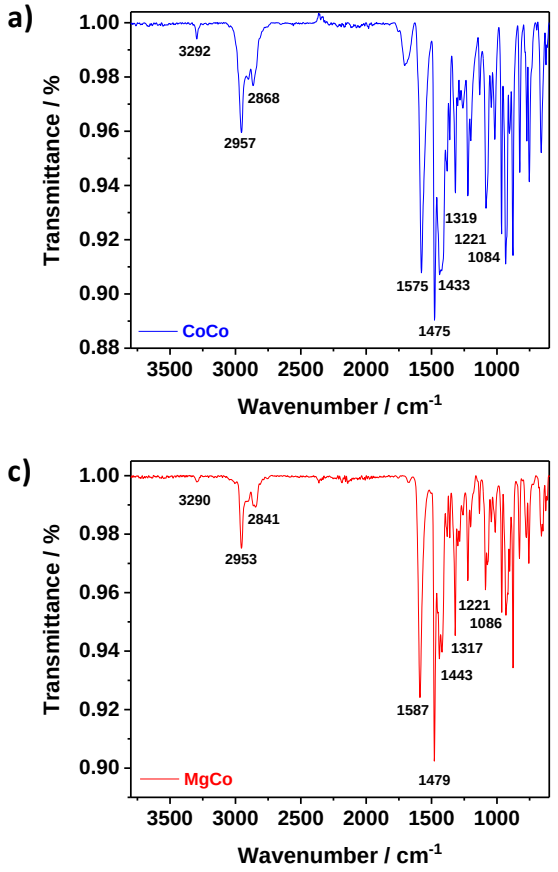


Figure 1: MALDI-ToF mass spectrum of **MgCo**.



Stretch	CoCo	MgCo	MgMg
N-H	3292	3290	3304
C-H (sp^2)	2957	2953	2949
C-H (sp^3)	2868	2841	2849
C=O (assym)	1575	1587	1593
C=C (Ar)	1475	1479	1481
C=O (sym)	1433	1443	1445
C-H bend	1319	1317	1313
C-N (ligand)	1221	1221	1223
C-O (phenol)	1084	1086	1070

Figure 2: FT-IR spectra of a) **CoCo**, b) **MgMg** and c) **MgCo**

X-ray Photoelectron Spectroscopy (XPS)

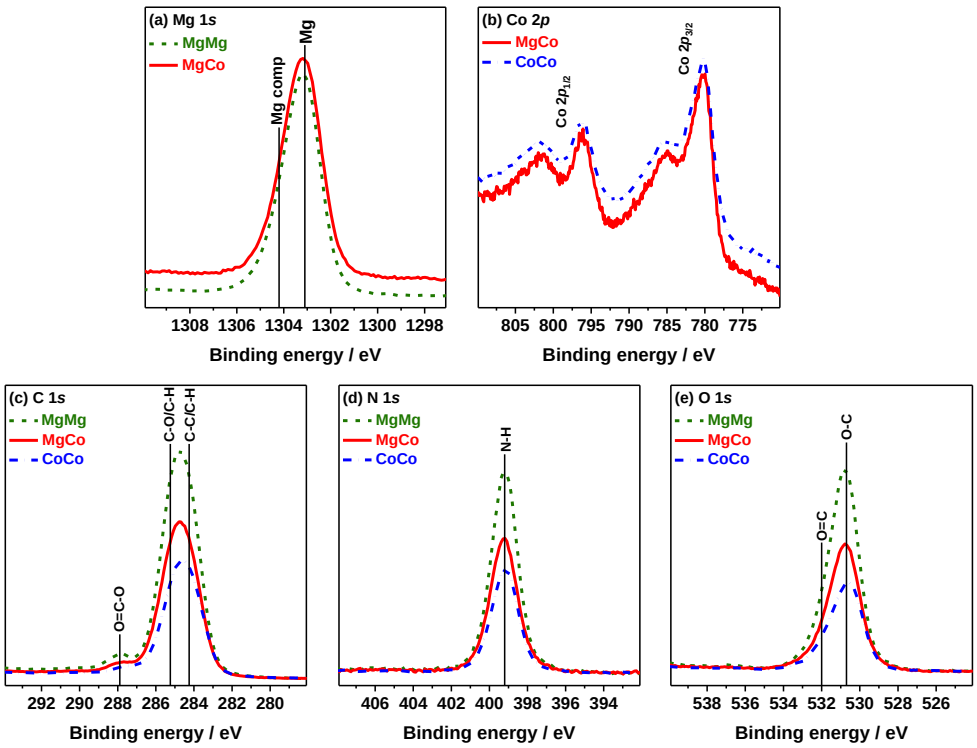


Figure 3: XPS core level spectra for the catalyst powders, including (a) Mg 1*s*, (b) Co 2*p*, (c) C 1*s*, (d) N 1*s* and (e) O 1*s*. The two metal core levels have standard normalisation and stacking applied to them, whilst the C, N and O 1*s* levels have been normalised to the total areas of the Mg and Co peaks.

In order to analyse the oxidation states of the Co(II) centres and the elemental composition of the catalysts, X-ray photoelectron spectroscopy (XPS) was used. Figure S2 shows the core levels of **MgMg**, **CoCo** and **MgCo**. The main metal core levels have been normalised and are shown as slightly stacked plots to avoid complete overlap. The Mg 1*s* core level shows a main contribution from the expected Mg environment of the catalyst at a binding energy (BE) of 1303.1 eV. The Co $2p_{1/2}$ and $2p_{3/2}$ core levels are observed in both **CoCo** and **MgCo** at a BE of 780.2 eV and 796.2 eV, respectively. In addition, satellite features 3-5 eV higher in BE (784.9 eV and 801.9 eV) are observed and are indicative for a Co(II) centre. From peak fitting of the Mg 1*s* and Co $2p_{3/2}$ core levels, a Mg:Co ratio of 1:1 was determined. The C 1s, N 1s, and O 1s core levels show all BE features expected from the structure of the catalyst such as C-O, C=O, C-C and N-H chemical environments.

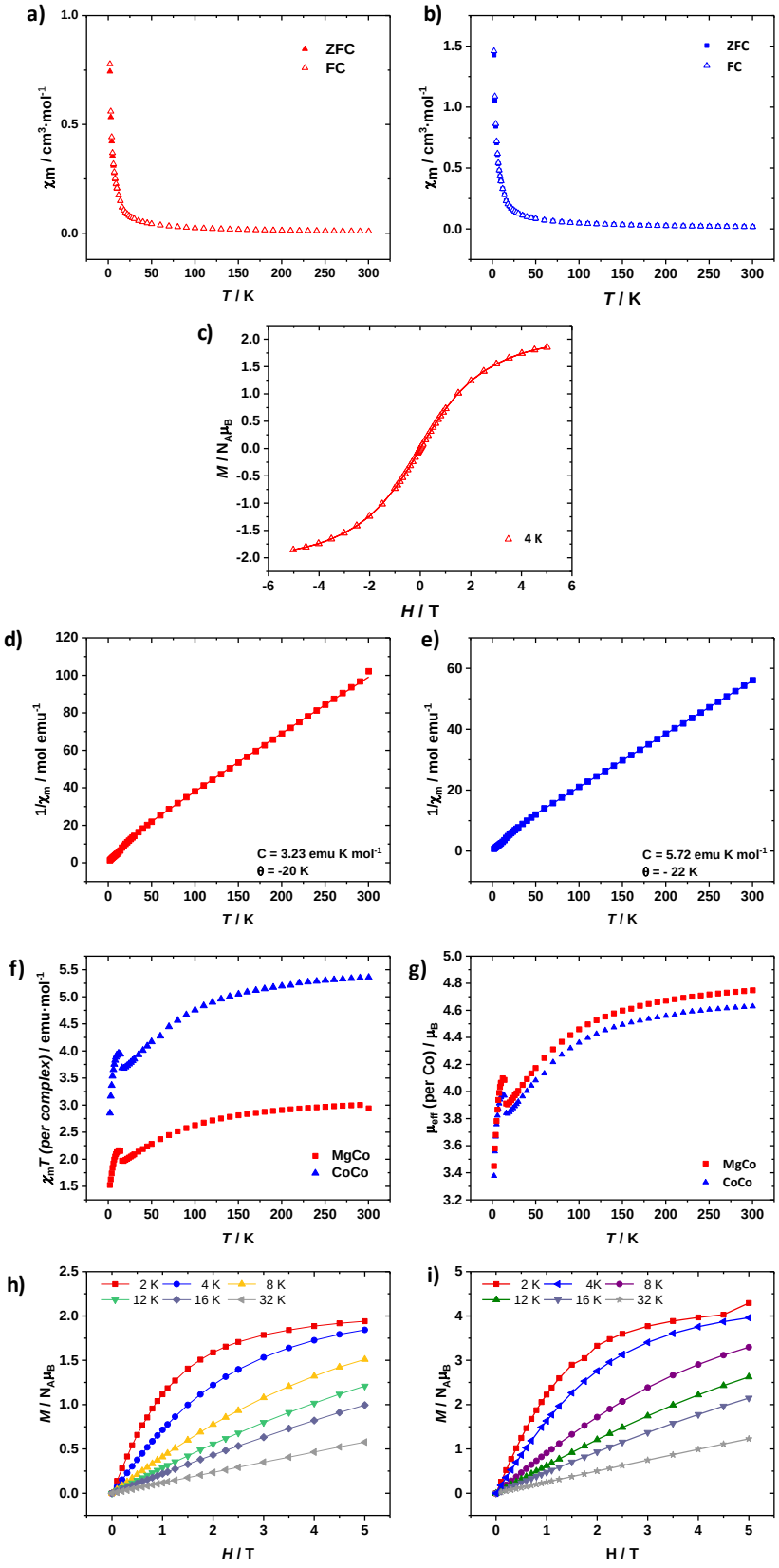


Figure 4: SQUID Magnetic data for **MgCo** and **CoCo**. Temperature dependence of the Field-Cooled (FC) and Zero-Field-Cooled (ZFC) magnetic susceptibilities of **MgCo** (a) and **CoCo** (b) per dinuclear complex at 0.1 Tesla. Curie-Weiss plot for **MgCo** (d) and **CoCo** (e). (f) Temperature dependence of observed $\chi_m T$ (per complex) for **MgCo** (■) and **CoCo** (▲) at 0.1 Tesla. (g) Temperature dependence of observed μ_{eff} per cobalt centre for **MgCo** (■) and **CoCo** (▲) at 0.1 Tesla. Magnetisation M vs. H plot (2-32 K) of **MgCo** (h) and **CoCo** (i) per dinuclear complex.

The magnetic susceptibility for both **MgCo** (Fig. S3a) and **CoCo** (Fig. S3b), per mole of dinuclear complex (χ_m), were identical for both zero-field cooled (ZFC) and field-cooled (FC) across all temperatures measured, indicating the complexes are magnetically dilute, hence only ZFC data are shown. Furthermore, no evidence was found for magnetic hysteresis for MgCo at 4 K (Fig. S3c).

The temperature dependence of the inverse of molar susceptibility, χ_m^{-1}, for both **MgCo** (Fig. S3d) and **CoCo** (Fig. S3e), are fitted by the linear Curie-Weiss law between 50 K and 300 K. A Curie constant, C, of 3.23 and 5.72 emu K mol^{-1} was determined for **MgCo** and **CoCo,** respectively. A negative Weiss temperature, θ, of ~ -21 K for both complexes indicates antiferromagnetic interactions.

At room temperature (300 K), the $\chi_m T$ product for **CoCo** is equal to 6.55 cm^3 mol^{-1} K and **MgCo** is equal to 2.82 cm^3 mol^{-1} K (Fig. S3f). Upon cooling, $\chi_m T$ decreases reaching a local minima at 18 K of 3.68 cm^3 mol^{-1} K for **CoCo** and 1.91 cm^3 mol^{-1} K for **MgCo**, which is followed by a sharp increase to attain a local maxima at 12 K of 3.96 cm^3 mol^{-1} K and 2.10 cm^3 mol^{-1} K for **CoCo** and **MgCo**, respectively. Below this temperature, $\chi_m T$ decreases abruptly to reach a minimum at 2 K of 3.85 cm^3 mol^{-1} K and 1.49 cm^3 mol^{-1} K for **CoCo** and **MgCo**, respectively. The decrease of $\chi_m T$ in the high temperature regime is due to the depopulation of the higher energy quartet and Kramer's doublet of the Co(II) ion. The increase in $\chi_m T$ on cooling after the local minimum at 12 K may be attributed to an intermolecular ferromagnetic interaction between the high-spin Co(II) ions in adjacent molecules. The final decrease of $\chi_m T$ at very low temperatures is due to intermolecular antiferromagnetic interactions and/or zero-field splitting effects of the ground state resulting from the antiparallel alignment of the interacting local spins.

The corresponding effective magnetic moments per cobalt ion (μ_{eff} per Co(II)) are 4.63 and 4.75 μ_B for **CoCo** and **MgCo**, respectively (Fig. S3g). These values are greater than the spin-only value for a high spin cobalt(II) centre (μ_{SO} = 3.87 μ_B for S= 3/2, g = 2), suggesting a significant spin-orbit coupling to the magnetic moment in both complexes. This is typically the case for high-spin Co(II) centres in an octahedral geometry due to the triple degeneracy of the ground state, $^4T_{1g}$.

Magnetic saturation is observed at 4.29 μ_B (2.15 μ_B per Co(II) centre) and 1.94 μ_B, for **CoCo** and **MgCo**, respectively (2 K, 5 Tesla, Fig. S3h-i). This result is in-line with several examples of Co(II) centred complexes reported, and is consistent with population of only the ground-state Kramers doublet at T < 30 K.[5-8]

Cyclic Voltammetry (CV):

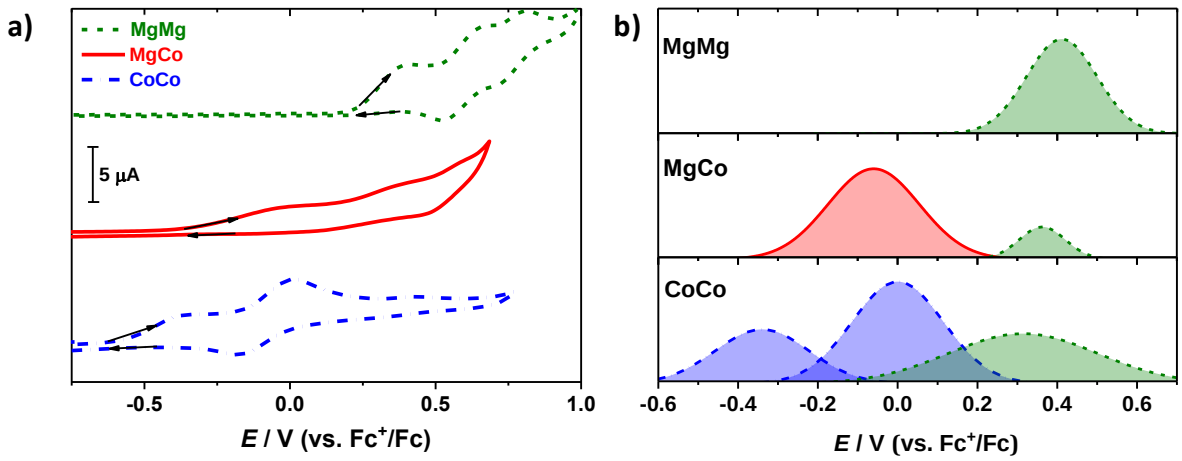


Figure 5: (a) Cyclic voltammagrams of **MgMg** (– –), **MgCo** (—), and **CoCo** (–•–) vs. Fc^+/Fc (THF, 0.1 M $[^nBu_4N][PF_6]$, 100 mV s^{-1}). (b) Oxidation potentials (E / V) of **MgMg**, **MgCo** and **CoCo** measured between -0.6 – 0.6 V vs. Fc^+/Fc. Solvent features have been subtracted and oxidation potentials have been deconvoluted resulting in the separation of ligand oxidation and Co(II) oxidations.

Table 1: Electrode potential (E) vs. $FeCp_2^{+/0}$ in THF

Complex	$E_{½}$ / V	E_{pp} / mV
MgMg	$E_{pa}^{(I)}$ = -0.02	-
	$E_{½}^{(II)}$ = +0.60	+0.24
	$E_{½}^{(III)}$ = +0.78	+0.21
MgCo	$E_{pa}^{(I)}$ = −0.03	-
	$E_{pa}^{(II)}$ = +0.41	-
CoCo	$E_{pa}^{(I)}$ = −0.37	-
	$E_{½}^{(II)}$ = −0.08	+0.21
	$E_{pa}^{(III)}$ =+0.42	-

CO_2/CHO Copolymerizations with and without 1,2-Cyclohexane Diol (CHD)

Table 2: CO_2/CHO copolymerizations using **MgCo** with and without additional 1,2-Cyclohexanediol (CHD).[a]

Entry	Cat. loading (mol %)	Stirring speed (RPM)	CHD (eq.)	Conv. (%)	TON [b]	TOF (h^{-1}) [c]	M_n [Đ] [d] (kg mol^{-1})
1	0.100	350	0	21	208	139	20.5 [1.27] 8.8 [1.13]
2	0.100	350	10	30	298	198	2.8 [1.14]
3	0.100	350	20	41	409	272	1.5 [1.12]
4	0.100	1400	20	51	510	340	2.0 [1.13]
5	0.050	1400	20	32	648	432	2.5 [1.11]
6	0.025	1400	20	15	606	404	2.5 [1.16]

[a]Copolymerization conditions: 80 °C, 1 bar CO_2, 90 mins, magnetic stirring. [b]Turnover number (TON) = number of moles of cyclohexene oxide consumed / number of moles of catalyst. [c]Turnover frequency (TOF) = TON / Time (h) for the overall reaction. [d]Determined by SEC, in THF, using narrow-M_n polystyrene standards as the calibrant; dispersity is given in brackets.

The optimisation of CO_2/CHO copolymerization reactions were carried out using **MgCo** at 80 °C, for 90 minutes, at 1 bar CO_2 pressure and in neat epoxide (9.9 M) (Table S2). All copolymerizations displayed both excellent CO_2 and polymer selectivity (> 99 %), with neither polyether linkages or cyclic carbonate observed by ^{1}H NMR spectroscopy. An initial study into the effects of adding chain transfer agent (CTA) was carried out using the bifunctional trans-1,2-cyclohexenediol (CHD) to form dihydroxy-terminated, telechelic polyols (entries 1-3). As the amount of CHD is increased from 0 to 20 equivalents (vs catalyst), the activity increased two-fold from 139 h^{-1} to 272 h^{-1}. The increased activity is attributed to the decrease in solution viscosity as a result of the formation of low molecular mass polyols (2 kg mol^{-1}). The activity was also increased by changing the stirring speed of the reaction from 350 RPM to 1400 RPM and this finding is attributed to mass transfer limitations at the lower stirring rate. To further reduce solution viscosity and find a region for kinetic analysis which was beyond the mass

transfer limit, the catalyst loading was reduced whilst maintaining CHD loading (Entry 4-6). A further increase in activity was observed upon decreasing the catalyst loading from 0.10 to 0.05 mol %. Decreasing the catalyst loading further to 0.025 mol % did not increase the rate of copolymerization further which indicated it is an appropriate set of conditions for study of reaction kinetics.

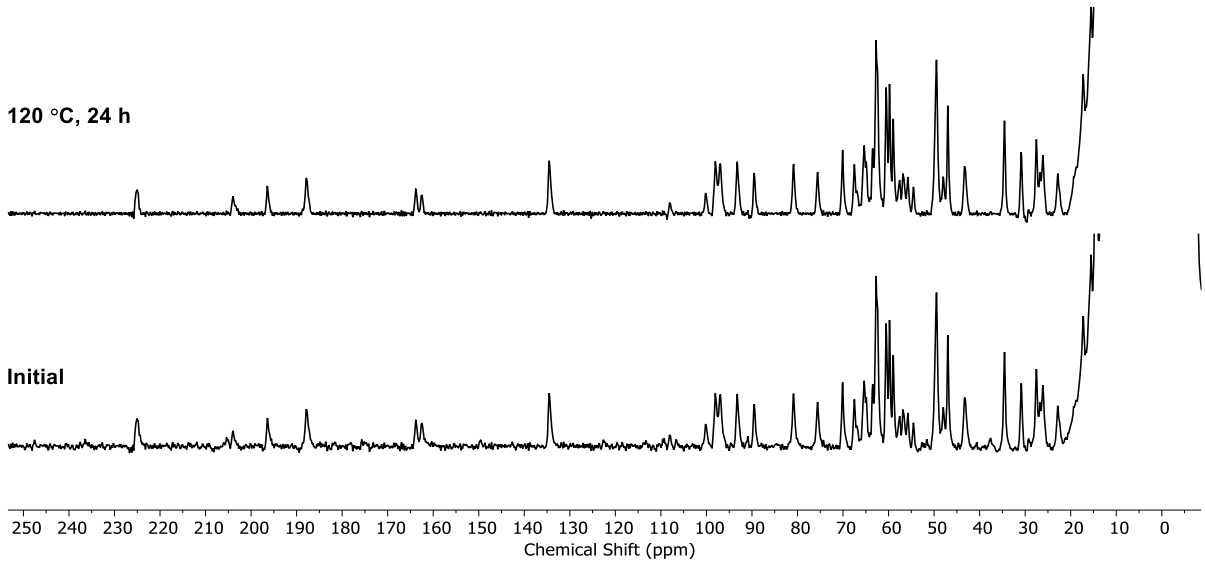


Figure 6: ^{1}H NMR spectra of **MgCo** before and after heating to 120 °C for 24 h in d_8-dioxane.

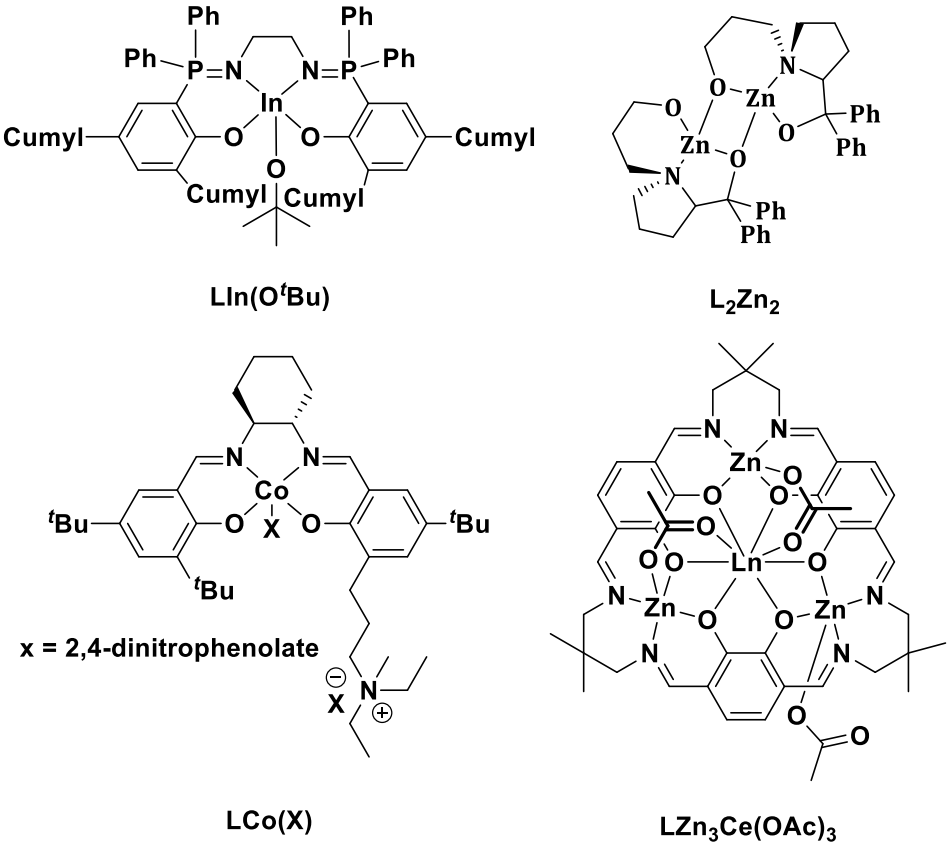


Figure 7: Molecular structures of other highly active 1 bar CO_2/CHO catalysts.[9-12]

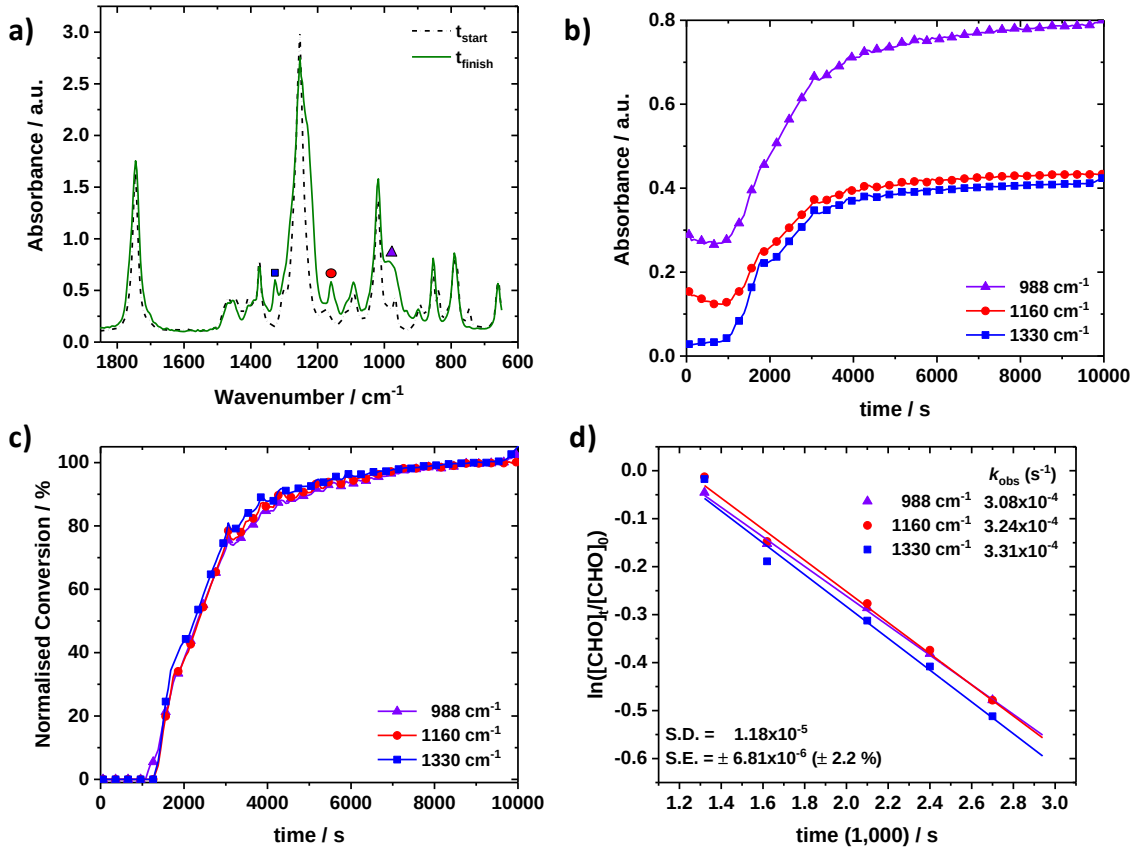


Figure 8: Copolymerization kinetic data (a) ReactIR spectra recorded at the start and finish of the copolymerization. Three peaks associated with PCHC were analysed: 988 (▲), 1160 (●) and 1330 cm^{-1} (■). (b) Absorbance vs. time plot for the three PCHC wavenumbers (every 5th data point displayed). (c) Normalised conversion vs. time plot for the three PCHC wavenumbers (every 5th data point displayed). (d) Logarithm of epoxide concentration vs. time for the three PCHC wavenumbers. k_{obs} (s^{-1}) values are reported and the average value used in subsequent analysis. Please note that the same induction period was observed regardless of the catalyst being tested (i.e. the induction period is not related to a particular catalyst structure).

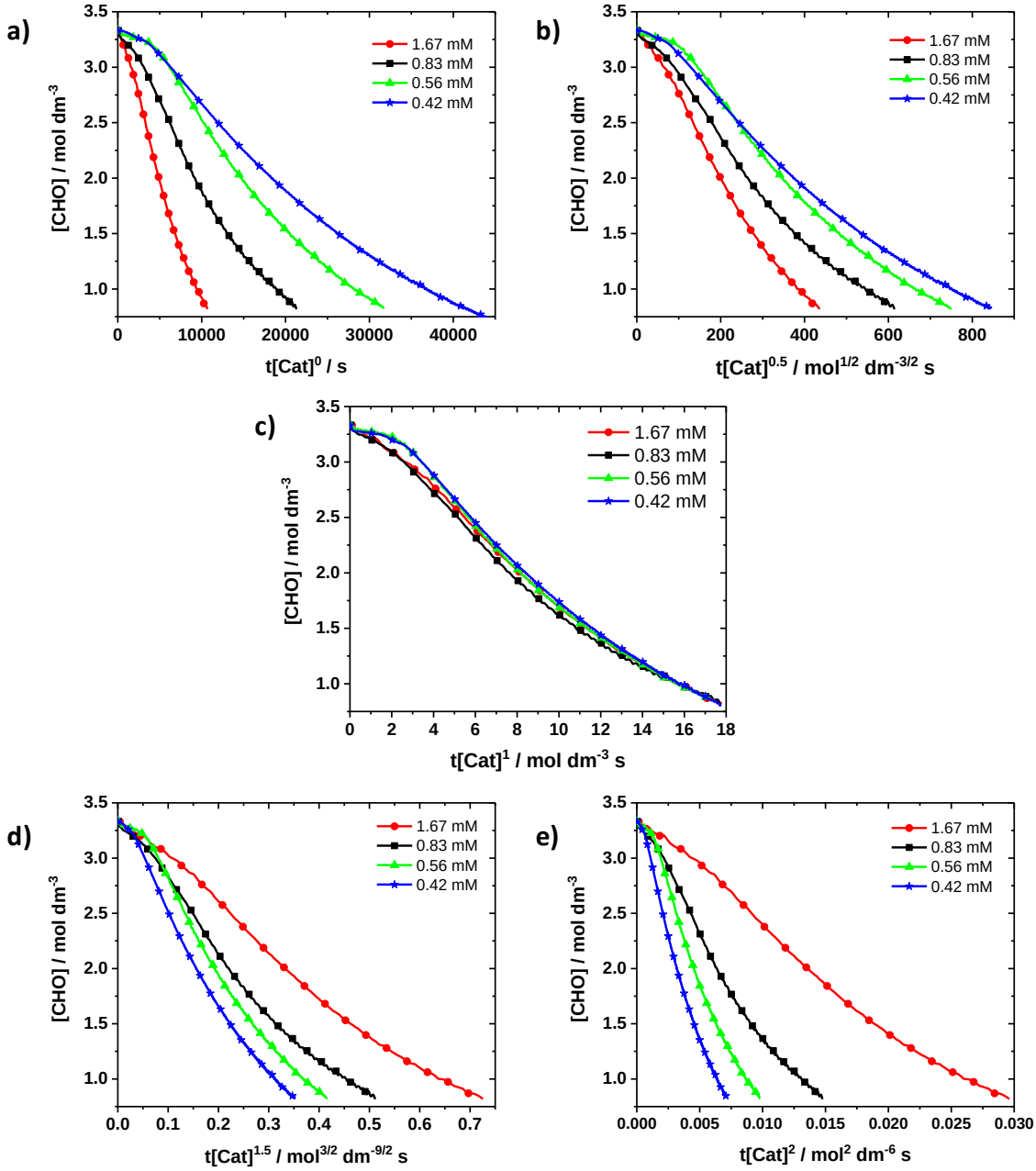


Figure 9: Reaction kinetic data; order in catalyst [**MgCo**] determined from a plot of [CHO] vs. t[cat]^{x}, where x = 0 (**a**), 0.5 (**b**), 1.0 (**c**), 1.5 (**d**) and 2.0 (**e**). Every 10th data point shown and plot correspond to 0-75 % conversion.

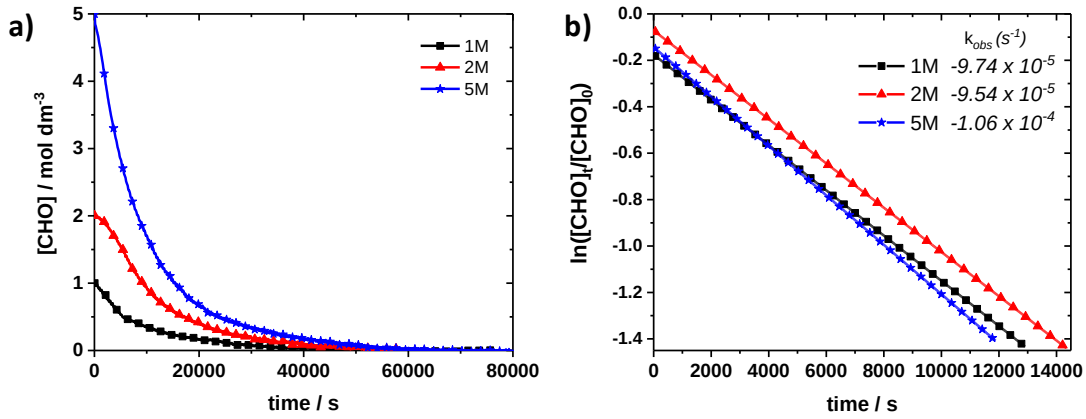


Figure 10: Kinetic analysis of ROCOP of CO_2/CHO using 1.67 mM MgCo in DEC (100 °C, 1 bar). (a) Plot of concentration [CHO] vs. time (s) plot for three epoxide concentrations: 1M (■), 2M (▲) and 5 M (★), every 30th data point presented. (b) Logarithm of concentration ($ln[CHO]_t/[CHO]_0$) vs. time (s) at three epoxide concentrations: 1M (■), 2M (▲) and 5M (★), every 30th data point presented.

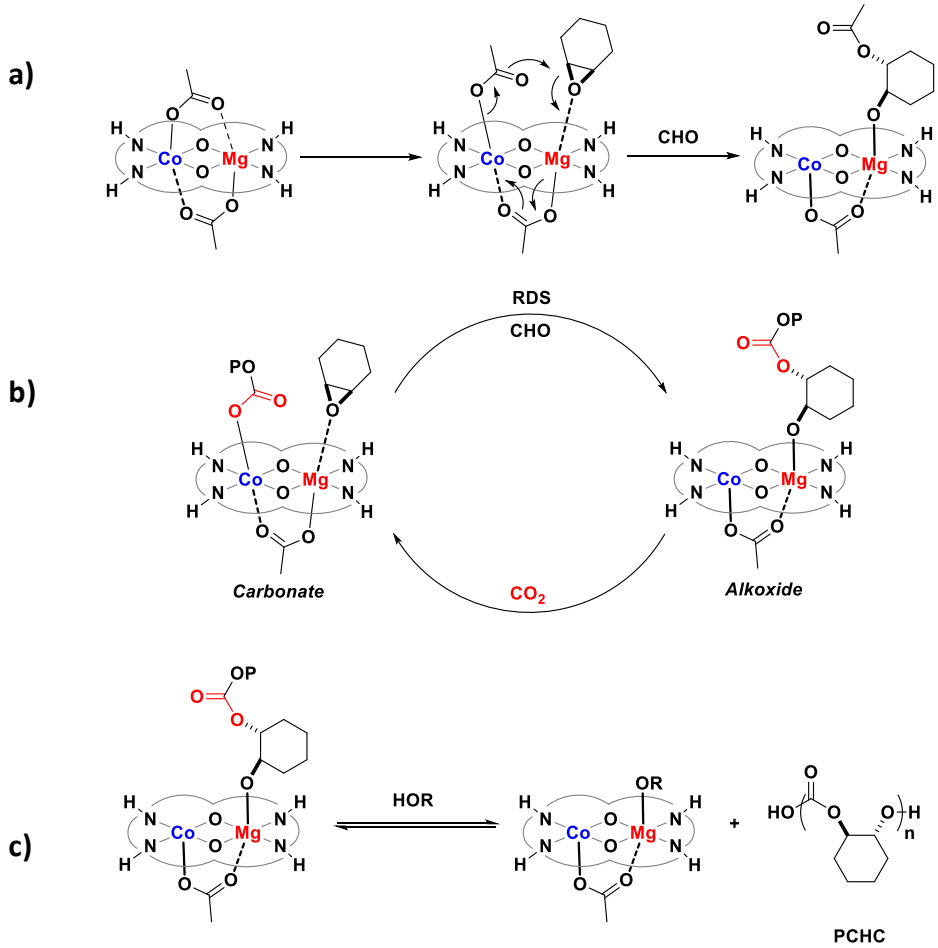


Figure 11. Proposed mechanisms for initiation (a), propagation (b) and chain-transfer (c).

Table 3: Effect of temperature on CO_2/CHO copolymerizations, at 1 bar CO_2.[a]

Entry	T (°C)	Time (h)	CO_2 (%)[b]	Polym. (%)[c]	TON[d]	TOF (PCHC) (h^{-1})[e]	TOF (CC) (h^{-1})
1	60	3.9	> 99	> 99	300	160	-
2	80	0.7	> 99	> 99	300	418	-
3	100	0.3	> 99	> 99	300	800	-
4	110	0.5	> 99	92	380	490	16
5	115	4.7	> 99	75	600	72	21
6	120	3.5	> 99	70	460	75	51
7	125	3.5	> 99	49	240	54	67

[a]Copolymerization conditions: 0.05 mol % cat, 20 equiv. 1,2-cyclohexane diol, 1 bar CO_2. [b]Expressed as a percentage of CO_2 uptake vs the theoretical maximum (100 %), determined by comparison of the relative integrals of the ^1H NMR resonances due to carbonate (δ 4.65 ppm) and ether (δ 3.45 ppm) linkages in the polymer backbone. [c]Expressed as a percentage of polymer formation vs. the theoretical maximum (100 %), determined by comparison of the relative integrals of the ^1H NMR proton resonances due to polymer (4.65 ppm), cis-cyclic carbonate (4.68 ppm) and trans-cyclic carbonate (4.00 ppm), with peak deconvolution applied as necessary. Note that cis and trans-cyclic carbonate isomers can be easily distinguished using IR spectroscopy. [d]Turnover number (TON) = number of moles of cyclohexene oxide consumed / number of moles of catalyst. [e]Turnover frequency (ToF) = TON / Time (h).

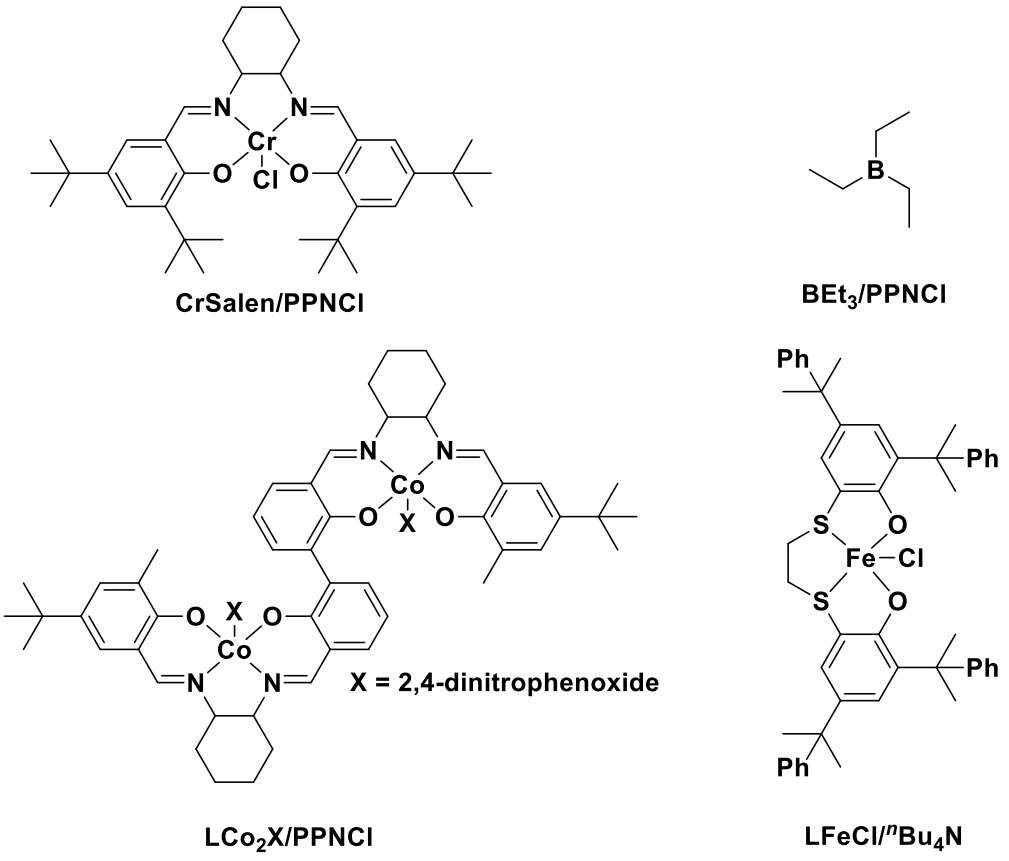


Figure 12: Molecular structures of other highly active CO_2/CHO catalysts (Elevated CO_2 Pressure).[13-16]

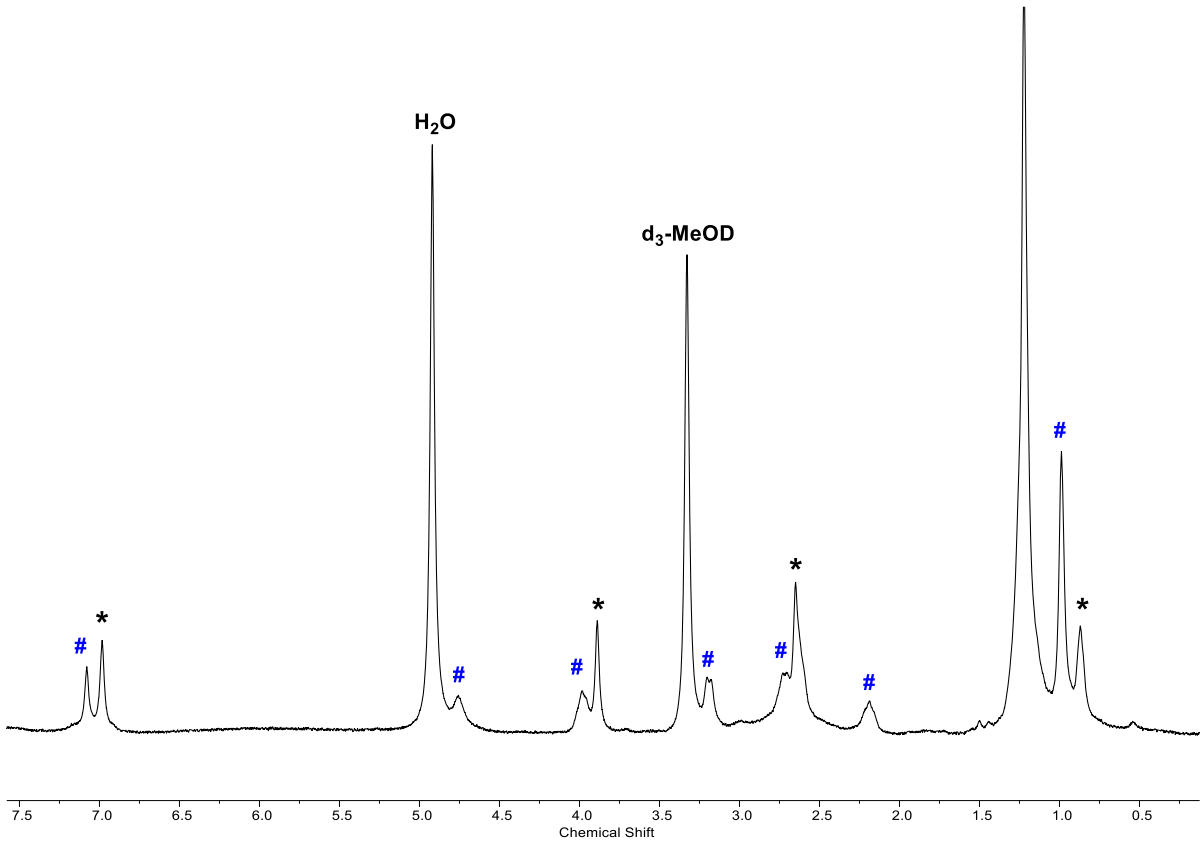


Figure 13: ^{1}H NMR spectrum of the product resulting from the attempted oxidation of **MgCo**. The spectrum shows the formation of protonated ligand (*) and MgMg (#).

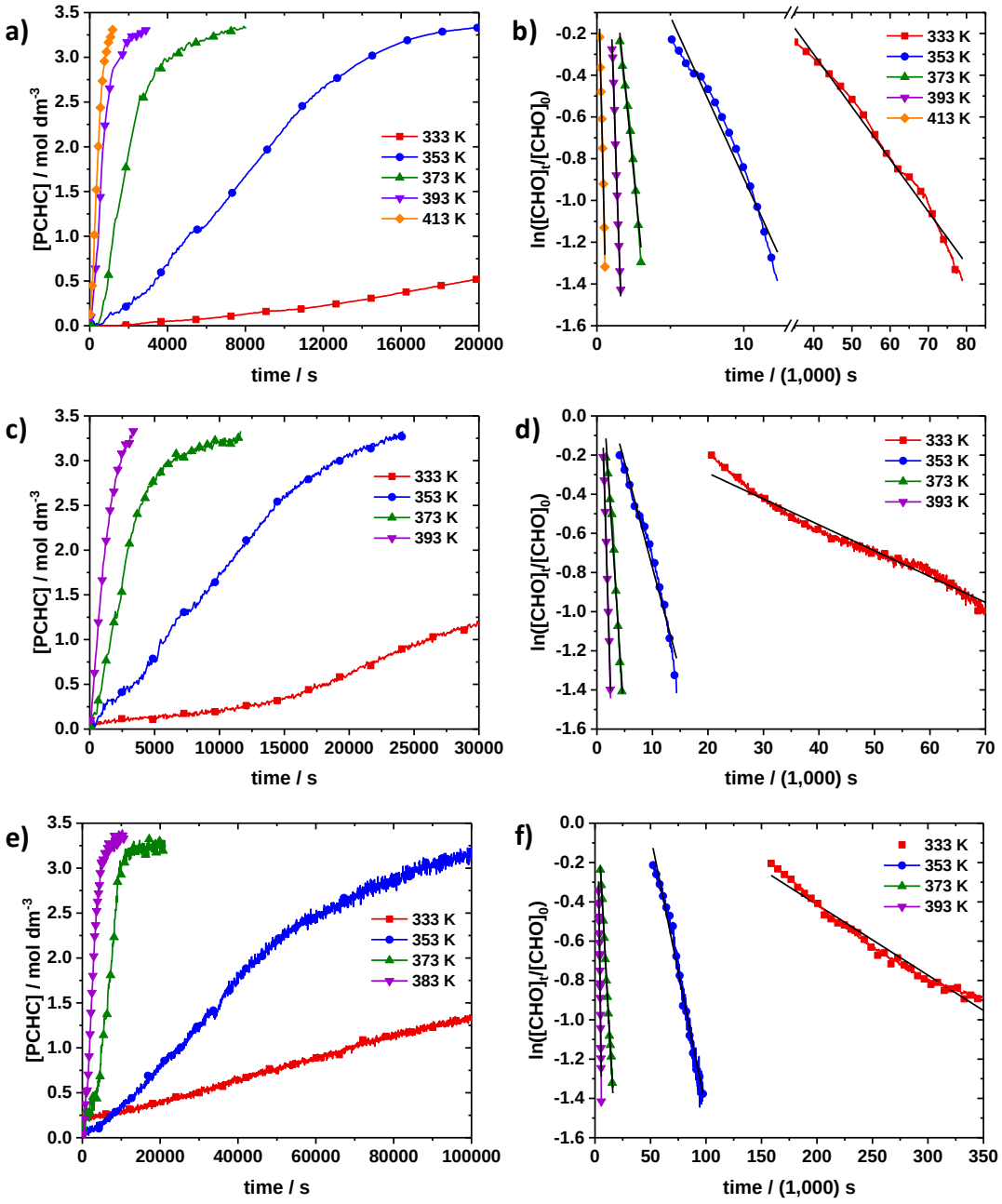


Figure 14. Temperature dependence of copolymerization rates. Conditions: 3.33 M CHO in DEC, 0.025 mol % cat, 20 eq 1,2-cyclohexene diol, 20 bar CO2. [PCHC] = 1-[CHO]. (a)/(c)/(d) Formation of PCHC vs time plots for **MgCo**, **CoCo** and **MgMg** at various temperatures. (b)/(d)/(f) Logarithm of CHO concentration vs time plot for **MgCo**, **CoCo** and **MgMg** at various temperatures.

Table 4: Data obtained from Eyring analysis, linear fits and calculated rate coefficients for the copolymerization of CO_2/CHO with **MgCo**.

Entry	T (K)	y = mx + c	R^2	k_{obs} (s^{-1})	k_p ($dm^3\ mol^{-1}\ s^{-1}$)	Ln(k/T)
1	333	$-2.51x10^{-5} + 0.71$	0.9928	$2.51x10^{-5}$ ($\pm 0.06x10^{-5}$)	0.0151 (±0.001)	-10.00 (±0.02)
2	353	$-1.55x10^{-4} + 0.65$	0.9810	$1.55x10^{-4}$ ($\pm 0.03x10^{-4}$)	0.0931 (±0.002)	-8.24 (±0.01)
3	373	$-7.14x10^{-4} + 0.92$	0.9933	$7.14x10^{-4}$ ($\pm 0.16x10^{-4}$)	0.4289 (±0.001)	-6.77 (±0.01)
4	393	$-2.05x10^{-3} + 1.87$	0.9972	$2.05x10^{-3}$ ($\pm 0.05x10^{-3}$)	1.2312 (±0.027)	-5.77 (±0.01)
5	413	$-2.98x10^{-3} + 0.36$	0.9949	$2.98x10^{-3}$ ($\pm 0.07x10^{-3}$)	1.7844 (±0.039)	-5.44 (±0.01)

k_{obs} = gradient of linear fitting of the logarithm of CHO concentration vs time. k = k_{obs}/[cat]^1 where [cat] = 1.67 mM. Errors from >2 repeat reactions in each case are ±2 %.

Table 5: Data obtained from Eyring analysis, linear fits and calculated rate coefficients for the copolymerization of CO_2/CHO with **CoCo**.

Entry	T (K)	y = mx + c	R^2	k_{obs} (s^{-1})	k_p ($dm^3\ mol^{-1}\ s^{-1}$)	Ln(k/T)
1	333	$-1.32x10^{-5} + 0.04$	0.9942	$1.32x10^{-5}$ ($\pm 0.03x10^{-5}$)	0.0079 (±0.001)	-10.65 (±0.02)
2	353	$-1.07x10^{-4} + 0.30$	0.9886	$1.07x10^{-4}$ ($\pm 0.02x10^{-4}$)	0.0931 (±0.003)	-8.61 (±0.01)
3	373	$-4.39x10^{-4} + 0.61$	0.9900	$4.39x10^{-4}$ ($\pm 0.10x10^{-4}$)	0.2637 (±0.007)	-7.23 (±0.01)
4	393	$-9.31x10^{-4} + 0.90$	0.9984	$9.31x10^{-4}$ ($\pm 0.20x10^{-4}$)	0.5592 (±0.012)	-6.56 (±0.01)

k_{obs} = gradient of linear fitting of the logarithm of CHO concentration vs time. k = k_{obs}/[cat]^1 where [cat] = 1.67 mM. Errors from >2 repeat reactions in each case are ±2 %.

Table 6: Data obtained from Eyring analysis, linear fits and calculated rate coefficients for the copolymerization of CO_2/CHO with **MgMg**.

Entry	T (K)	y = mx + c	R^2	k_{obs} (s^{-1})	k_p ($dm^3\ mol^{-1}\ s^{-1}$)	Ln(k/T)
1	333	$-3.58x10^{-6} + 0.30$	0.9837	$3.58x10^{-6}$ ($\pm 0.08x10^{-6}$)	0.0022 (±0.0005)	-11.95 (±0.02)
2	353	$-2.78x10^{-5} + 1.33$	0.9938	$2.78x10^{-5}$ ($\pm 0.06x10^{-5}$)	0.0167 (±0.0004)	-9.96 (±0.02)
3	373	$-1.02x10^{-4} + 0.27$	0.9989	$1.02x10^{-4}$ ($\pm 0.02x10^{-4}$)	0.0613 (±0.0017)	-8.71 (±0.01)
4	393	$-4.49x10^{-4} + 0.54$	0.9765	$4.49x10^{-4}$ ($\pm 0.10x10^{-4}$)	0.2697 (±0.008)	-7.28 (±0.01)

k_{obs} = gradient of linear fitting of the logarithm of CHO concentration vs time. k$_p$ = k_{obs}/[cat]^1 where [cat] = 1.67 mM. Errors from >2 repeat reactions in each case are ±2 %.

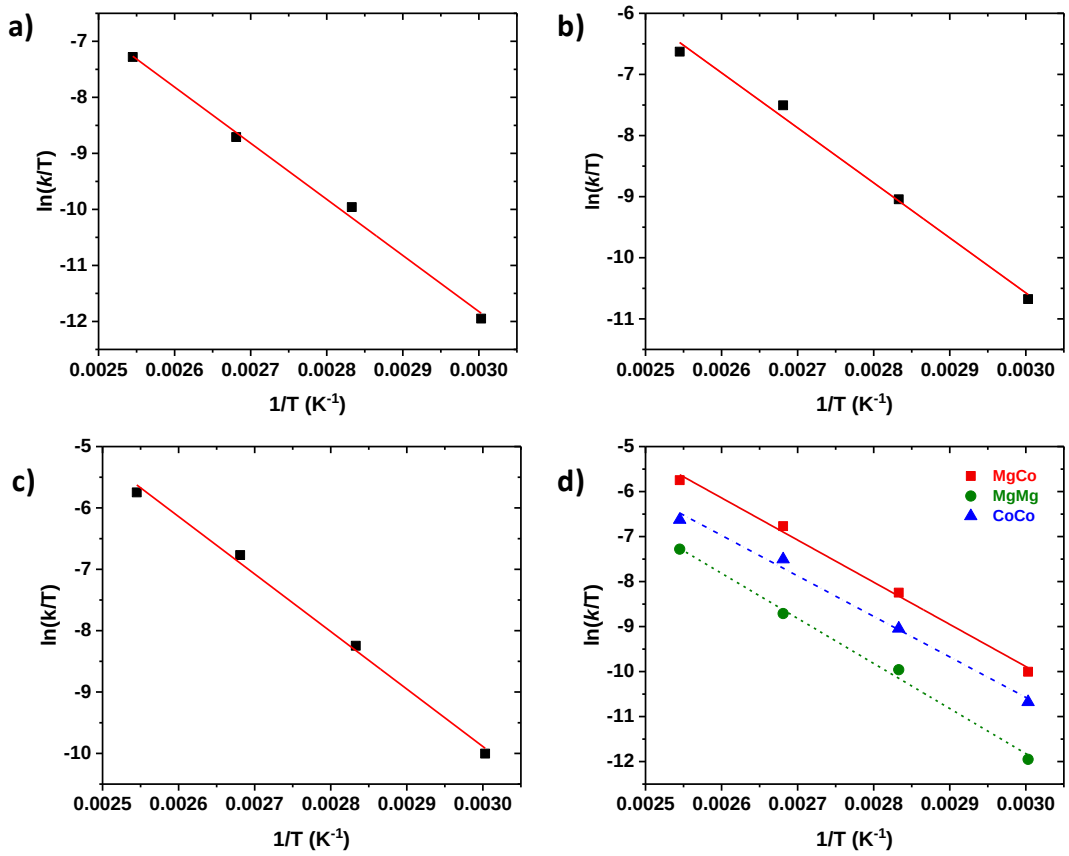


Figure 15: Eyring plots (ln(k/T) vs 1/T) for **MgCo** (a), **CoCo** (b) and **MgMg** (c), respectively. (d) Combined Eyring Analysis for **MgCo (■)**, **CoCo(▲)** and **MgMg(●)**.

Table 7: Transition state themodynamic parameters, $\Delta H^{\ddagger}$ and $\Delta S^{\ddagger}$, determined *via* the Eyring analysis.

Entry	Cat.	y = mx + c	R^2	$\Delta H^{\ddagger}$ (kJ mol^{-1})	$\Delta S^{\ddagger}$ (J mol^{-1} K^{-1})	$\frac{\sigma(\Delta S^{\ddagger})}{\sigma(\Delta H^{\ddagger})} \approx \frac{1}{T_{av}}$
1	**MgMg**	10090x + 18.41	0.9978	83.3(±1.3)	-45.4(±3.7)	0.00285
2	**CoCo**	9002x + 16.43	0.9965	74.9(±1.5)	-60.2(±4.2)	0.00280
3	**MgCo**	9308x + 18.21	0.9978	77.3(±1.2)	-46.1(±3.4)	0.00283

Errors calculated using Least Squares Fitting Analysis.

Table 8: CO_2/Other epoxide ROCOP using **MgCo**.[a]

#	Epoxide	CO_2 (%)	Poly. (%)[b]	TON[c]	TOF (h^{-1})[d]	k_p ($dm^3\ mol^{-1}\ s^{-1}$)[e]	M_n (kg mol^{-1}) [Đ][f]
1	CHO	> 99	> 99	320	3200	0.4289	2.8 [1.14]
2	vCHO	> 99	> 99	290	2900	0.4069	2.0 [1.13]
3	LO	-	-	-	-	-	*n.d*
4	CPO[g]	> 99	91	300	214	0.0255	3.3 [1.24]
5	PO[h]	97	2	125	5	-	*n.d*

[a]Copolymerization conditions: cat : CHO 0.05 mol %, 20 eq. CHD, 20 bar CO_2, 3M epoxide concentration in DEC (total volume 10 mL) 100 °C unless stated otherwise. All entries report >99 CO_2 selectivity vs. theoretical maximum (100 %). CHO: cyclohexene oxide, vCHO: 4-vinyl-1,2-cyclohexene oxide LO: Limonene oxide, E-THF: 3,4-epoxytetrahydrofuran, CPO: cyclopentene oxide, PO: propylene oxide, AGE: allyl gylcidyl ether. [g]9% cis-cyclic carbonate. [h]Copolymerization conditions: cat: PO 0.1 mol %, 20 eq CHD, 20 bar CO_2, neat PO (14 M), 60°C, below 60 °C resulted in trace conversions.

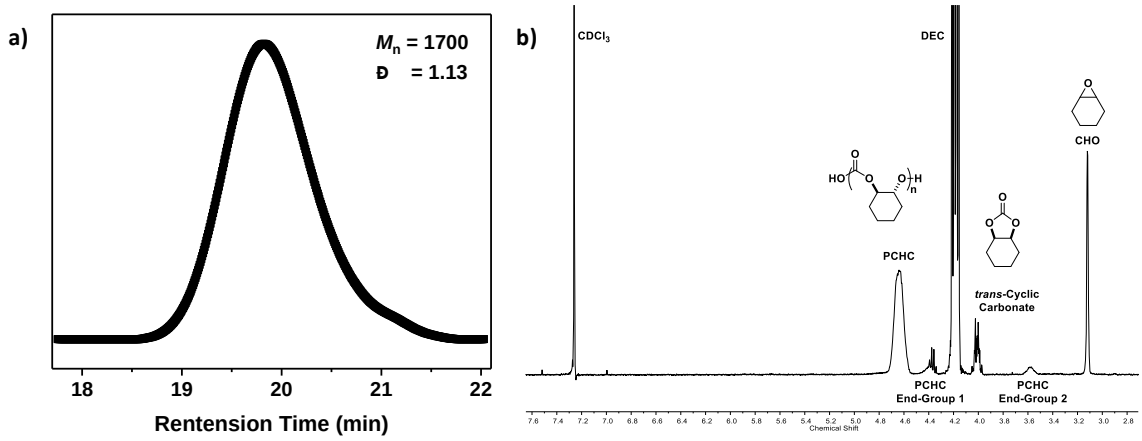


Figure 16: Representative examples of a) GPC Analysis and b) ^1H NMR spectra of the crude polymers.

References

1. Kember, M. R.; White, A. J. P.; Williams, C. K., Highly Active Di- and Trimetallic Cobalt Catalysts for the Copolymerization of CHO and CO_2 at Atmospheric Pressure*, Macromolecules,* **2010,** *43*, (5), 2291.
2. Kember, M. R.; Williams, C. K., Efficient Magnesium Catalysts for the Copolymerization of Epoxides and CO_2; Using Water to Synthesize Polycarbonate Polyols*, J. Am. Chem. Soc.,* **2012,** *134*, (38), 15676.
3. Kember, M. R.; Knight, P. D.; Reung, P. T. R.; Williams, C. K., Highly Active Dizinc Catalyst for the Copolymerization of Carbon Dioxide and Cyclohexene Oxide at One Atmosphere Pressure*, Angew. Chem. Int. Ed.,* **2009,** *48*, (5), 931.
4. Bain, G. A.; Berry, J. F., Diamagnetic Corrections and Pascal's Constants*, J. Chem. Educ.,* **2008,** *85*, (4), 532.
5. Rodriguez, A.; Sakiyama, H.; Masciocchi, N.; Galli, S.; Gálvez, N.; Lloret, F.; Colacio, E., Hexacyanocobaltate(III) Anions as Precursors of Co(II)–Ni(II) Cyano-Bridged Multidimensional

Assemblies: Hydrothermal Syntheses, Crystal and Powder X-ray Structures, and Magnetic Properties, *Inorg. Chem.,* **2005,** *44*, (23), 8399.
6. Mishra, V.; Lloret, F.; Mukherjee, R., Coordination versatility of 1,3-bis[3-(2-pyridyl)pyrazol-1-yl]propane: Co(II) and Ni(II) complexes, *Inorg. Chim. Acta,* **2006,** *359*, (12), 4053.
7. Herrera, J. M.; Bleuzen, A.; Dromzée, Y.; Julve, M.; Lloret, F.; Verdaguer, M., Crystal Structures and Magnetic Properties of Two Octacyanotungstate(IV) and (V)-Cobalt(II) Three-Dimensional Bimetallic Frameworks, *Inorg. Chem.,* **2003,** *42*, (22), 7052.
8. Du, K.; Thorarinsdottir, A. E.; Harris, T. D., Selective Binding and Quantitation of Calcium with a Cobalt-Based Magnetic Resonance Probe, *J. Am. Chem. Soc.,* **2019,** *141*, (17), 7163.
9. Thevenon, A.; Cyriac, A.; Myers, D.; White, A. J. P.; Durr, C. B.; Williams, C. K., Indium Catalysts for Low-Pressure CO_2/Epoxide Ring-Opening Copolymerization: Evidence for a Mononuclear Mechanism?, *J. Am. Chem. Soc.,* **2018,** *140*, (22), 6893.
10. Mike, S.; Sebastian, D.; Franc, M., Highly Active and Readily Accessible Proline-Based Dizinc Catalyst for CO2/Epoxide Copolymerization, *Chem. Eur. J.,* **2017,** *23*, (65), 16472.
11. Nagae, H.; Aoki, R.; Akutagawa, S.; Kleemann, J.; Tagawa, R.; Schindler, T.; Choi, G.; Spaniol, T. P.; Tsurugi, H.; Okuda, J.; Mashima, K., Lanthanide Complexes Supported by a Trizinc Crown Ether as Catalysts for Alternating Copolymerization of Epoxide and CO_2: Telomerization Controlled by Carboxylate Anions, *Angew. Chem. Int. Ed.,* **2018,** *57*, (9), 2492.
12. Ren, W.-M.; Zhang, X.; Liu, Y.; Li, J.-F.; Wang, H.; Lu, X.-B., Highly Active, Bifunctional Co(III)-Salen Catalyst for Alternating Copolymerization of CO2 with Cyclohexene Oxide and Terpolymerization with Aliphatic Epoxides, *Macromolecules,* **2010,** *43*, (3), 1396.
13. Li, J.; Liu, Y.; Ren, W.-M.; Lu, X.-B., Asymmetric Alternating Copolymerization of Meso-epoxides and Cyclic Anhydrides: Efficient Access to Enantiopure Polyesters, *J. Am. Chem. Soc.,* **2016,** *138*, (36), 11493.
14. Darensbourg, D. J.; Mackiewicz, R. M.; Billodeaux, D. R., Pressure Dependence of the Carbon Dioxide/Cyclohexene Oxide Coupling Reaction Catalyzed by Chromium Salen Complexes. Optimization of the Comonomer-Alternating Enchainment Pathway, *Organometallics,* **2005,** *24*, (1), 144.
15. Liu, Y.; Ren, W.-M.; Liu, J.; Lu, X.-B., Asymmetric Copolymerization of CO2 with meso-Epoxides Mediated by Dinuclear Cobalt(III) Complexes: Unprecedented Enantioselectivity and Activity, *Angew. Chem. Int. Ed.,* **2013,** *52*, (44), 11594.
16. Della Monica, F.; Maity, B.; Pehl, T.; Buonerba, A.; De Nisi, A.; Monari, M.; Grassi, A.; Rieger, B.; Cavallo, L.; Capacchione, C., [OSSO]-Type Iron(III) Complexes for the Low-Pressure Reaction of Carbon Dioxide with Epoxides: Catalytic Activity, Reaction Kinetics, and Computational Study, *ACS Catal.,* **2018,** 6882.